The EMBO Journal vol.15 no.17 pp.4643–4653, 1996

Localization of yeast RNA polymerase I core subunits by immunoelectron microscopy

Corinne Klinger, Janine Huet[1], Danying Song[2], Gabriele Petersen[2], Michel Riva[1], Ekkehard K.F.Bautz[2], André Sentenac[1], Pierre Oudet and Patrick Schultz

Institut de Génétique et de Biologie Moléculaire et Cellulaire, 1, rue Laurent Fries, BP163 F-67404 Illkirch Cedex, [1]Service de Biochimie et Génétique Moléculaire, Centre d'Etudes de Saclay, F-91191 Gif sur Yvette cedex, France and [2]Institute for Molecular Genetics, University of Heidelberg, Im Neuenheimer Feld 230, D-69120 Heidelberg, Germany

Immunoelectron microscopy was used to determine the spatial organization of the yeast RNA polymerase I core subunits on a three-dimensional model of the enzyme. Images of antibody-labeled enzymes were compared with the native enzyme to determine the localization of the antibody binding site on the surface of the model. Monoclonal antibodies were used as probes to identify the two largest subunits homologous to the bacterial β and β′ subunits. The epitopes for the two monoclonal antibodies were mapped using subunit-specific phage display libraries, thus allowing a direct correlation of the structural data with functional information on conserved sequence elements. An epitope close to conserved region C of the β-like subunit is located at the base of the finger-like domain, whereas a sequence between conserved regions C and D of the β′-like subunit is located in the apical region of the enzyme. Polyclonal antibodies outlined the α-like subunit AC_{40} and subunit AC_{19} which were found co-localized also in the apical region of the enzyme. The spatial location of the subunits is correlated with their biological activity and the inhibitory effect of the antibodies.

Keywords: epitope localization/image analysis/ immunoelectron microscopy/subunits/yeast RNA polymerase I (A)

Introduction

DNA-dependent RNA polymerases form a family of multisubunit enzymes present in all living organisms and essential for gene expression. Eukaryotes make use of three distinct forms of enzyme to synthesize rRNA precursors (enzyme I or A), pre-mRNA (enzyme II or B) and small RNAs like tRNA and 5S RNA (enzyme III or C). Primary sequence analysis and functional homologies suggest that the $\alpha_2\beta\beta'$ subunit composition of the bacterial core enzyme is shared by all RNA polymerases and thus contains most of the catalytic activities. Regions with substantial sequence conservation, termed homology regions, were identified between the prokaryotic β′ and β subunits and the largest (Allison *et al.*, 1985; Corden *et al.*, 1985; Mémet *et al.*, 1988) and the second largest subunits (Sweetzer *et al.*, 1987; James *et al.*, 1991; Yano and Nomura, 1991) respectively of eukaryotes and archeabacteria (for a review, see Thuriaux and Sentenac, 1992).

Five homology regions (c, d, f, g and h) are found in all β′-like subunits. Regions a and b are not strictly conserved in the eubacterial subunit, but the zinc binding properties of region a are preserved (Treich *et al.*, 1991). The β′-like subunit is believed to bind RNA in region g (Coulter and Greenleaf, 1985; Borukhov *et al.*, 1991; Hekmatpanah and Young, 1991) and probably in region d which was proposed to participate in the active site (Dieci *et al.*, 1995). In addition, α-amanitin, which specifically blocks RNA chain elongation, interacts with region f (Bartolomei and Corden 1987; de Mercoyrol *et al.*, 1989). This subunit also participates in DNA binding as shown by blotting experiments, UV cross-linking (Gundelfinger, 1983; Bartholomew *et al.*, 1993; Kontermann *et al.*, 1993), functional inhibition by subunit-specific antibodies (Bréant *et al.*, 1983) and changes in protease susceptibility (Horikoshi *et al.*, 1985).

Eight regions (from B to I), are conserved in the sequences of all β-like subunits so far analyzed. Domain J, which contains a zinc binding motif, and domain A are found only in eukaryotic nuclear enzymes and in archeabacteria. Affinity labeling experiments show that the initiator nucleotide binding site is located in the β-like subunit in prokaryotes (Grachev *et al.*, 1987) and in yeast (Riva *et al.*, 1987). This site was mapped precisely within the conserved domains H and I (Grachev *et al.*, 1989; Treich *et al.*, 1992). The sequences encompassing domains C and D affect chain termination (James *et al.*, 1991) and may cause altered pausing (Landick *et al.*, 1990), and are therefore believed to interact with RNA. Cross-linking experiments indicate that this subunit also contacts the DNA template (Gundelfinger, 1983; Bartolomew *et al.*, 1993). Non-specific DNA binding sites were revealed within domains C and D of *Drosophila melanogaster* RNA polymerase II by South-Western analysis (Kontermann and Bautz, 1994).

Besides the large subunits which contain most of the catalytic activities, interest is growing in the α-like subunit present as a dimer in the *Escherichia coli* enzyme. In addition to the originally assessed function in enzyme assembly (Yura and Ishihama, 1979), the α subunit contacts DNA and plays a role in the control of RNA polymerase activity (Igarashi and Ishihama, 1991; Kolb *et al.*, 1993; Ross *et al.*, 1993; Blatter *et al.*, 1994). On the basis of size and sequence homologies, common stoichiometry and similar function in enzyme assembly, the B_{44} subunit was identified as the yeast RNA polymerase II equivalent of α (Kolodziej and Young, 1989) the subunit nomenclature identifies the yeast enzyme class to which it belongs, A

(I), B (II) and C (III), and the apparent size of the polypeptide in kDa$\times 10^{-3}$]. In class I and III enzymes, the AC_{40} subunit has functional and sequence similarities with α and with B_{44} (Mann *et al.*, 1987; Martindale, 1990) but its stoichiometry is not firmly established. The AC_{19} subunit shares local sequence similarities with the amino-terminal region of α (Dequard-Chablat *et al.*, 1991) and is believed to interact with AC_{40} (Lalo *et al.*, 1993). A homologous polypeptide is associated with yeast RNA polymerase II (Woychik *et al.*, 1993).

Electron microscopy has so far provided the most accurate structural description of the enzyme mainly through the development of two-dimensional crystallization methods on charged lipid layers (Darst *et al.*, 1989, 1991a; Schultz *et al.*, 1993). The three-dimensional models determined for the *E.coli* and the yeast class I and II enzymes share common structural features such as their size of ~11 nm×11 nm×15 nm, the presence of a 3 nm wide and 10 nm long groove, and a finger-like domain which partially occludes the groove and forms a 2.5 nm wide channel. RNA polymerase subunit-specific antibodies were used successfully as structural probes to demonstrate antigenic cross-reactivities between the large subunits of the various enzymes (Buhler *et al.*, 1980; Huet *et al.*, 1982b, 1983, 1985). These antibodies were also used as functional probes to block specific steps of the enzymatic reaction such as RNA chain elongation (Rose *et al.*, 1983), template binding (Huet *et al.*, 1982a; Bréant *et al.*, 1983) or the differential inhibition in a specific versus a non-specific transcription system (Huet *et al.*, 1985). An inhibitory effect due to the binding of an antibody molecule may result from the proximity of the epitope and the active site or from a long distance steric effect on substrate binding. The localization of the antibody binding site on a spatial model of the enzyme would therefore shed some light on the mechanism of inhibition and provide structural information on the quaternary organization of the enzyme.

This study describes the localization of four enzyme subunits on the three-dimensional model of yeast RNA polymerase I using polyclonal or monoclonal antibodies. The epitopes recognized by the monoclonal antibodies were mapped on the primary sequence by using subunit-specific phage display libraries. Immune complexes were adsorbed directly on carbon or lipid supports and observed as isolated particles. This direct method was used widely to study the quaternary structure of large macromolecular assemblies (Tichelaar *et al.*, 1983; Lotti *et al.*, 1989; Boisset *et al.*, 1993). Numerical image analysis methods were used to calculate statistically significant average images representing characteristic views of the labeled enzyme in order to identify the probe, to detect precisely its interaction site and to demonstrate the binding specificity. The spatial locations of the antibody binding sites were deduced from at least two different labeled enzyme views. The β-like epitope was found close to the finger-like stalk and at the outside of the groove. The β′-like epitope is located near the dimerization interface of the enzyme and close to the AC_{40} and AC_{19} subunits, which are co-localized in the apical region of the enzyme. The position of the subunits is discussed with regard to the effect of the antibodies on the enzymatic activity.

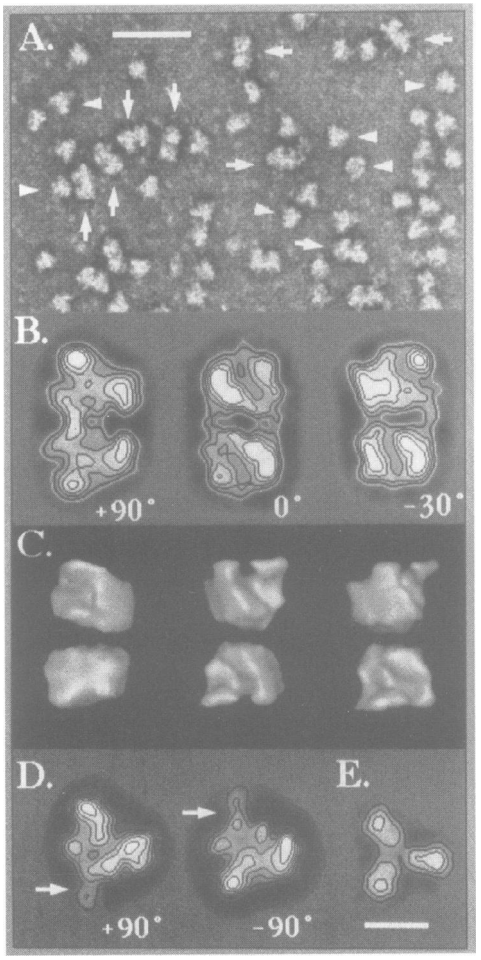

Fig. 1. Characteristic views of unlabeled yeast RNA polymerase I and of unbound IgG molecules. (**A**) Scanning transmission electron micrograph of RNA polymerase molecules adsorbed on a carbon film and negatively stained with uranyl acetate showing the monomeric (arrowheads) and dimeric (arrows) forms of the enzyme. The bar represents 50 nm. (**B**) Gallery of the most representative RNA polymerase dimer views obtained upon averaging the aligned images, clustered into homogeneous classes. The stain-excluding protein densities are represented in white and are outlined by contours of equal density. The three views correspond to different orientations of the dimeric enzyme related to each other by a rotation around the long dimer axis. The rotation angle, which is indicated for each projection, is referenced to the orientation where the 2-fold symmetry axis is normal to the supporting film. (**C**) Surface representation of the three-dimensional RNA polymerase dimer model (Schultz *et al.*, 1993) oriented so as to correspond to the views represented in (B). (**D**) Average views of the monomeric RNA polymerase corresponding to two reversed orientations on the supporting film. When these two monomer projections are associated by superposing the two arrows, the 90° dimer view is formed (B), thus indexing the orientation of the monomer views. This analysis revealed an additional protein density present in the dimerization interface (arrows). (**E**) Average projection of an IgG molecule obtained after alignement of 353 antibody images. A large variability was detected in the hinge region upon clustering of the aligned images (data not shown). The bar indicates 10 nm in (B–E).

Results

Native RNA polymerase projections

When purified enzyme molecules are adsorbed on a carbon film and are negatively stained, dimeric and monomeric enzyme forms are clearly distinguished by their size of ~11×20 nm and 11×15 nm, respectively (Figure 1A). In buffer A, 60% of the polymerases were organized as

Table I. Statistics of the image data sets for antibody-labeled RNA polymerase dimers

Subunit-specific probe	Dimer view as defined in Figure 1	No. of images analyzed	Putatively labeled dimers	Specifically labeled dimers
A_{135}	90°	300	97 (32%)	62 (64%)
	0°	45	n.d.	n.d.
	–30°	133	49 (37%)	41 (84%)
	others	122	n.d.	n.d.
AC_{40}	90°	197	144 (73%)	90 (63%)
	0°	34	n.d.	n.d.
	–30°	144	49 (34%)	37 (75%)
	others	87	n.d.	n.d.
AC_{19}	90°	224	116 (52%)	90 (77%)
	0°	37	14 (38%)	9 (64%)
	–30°	58	n.d.	n.d.
	others	82	n.d.	n.d.

dimers, whereas this percentage was reduced to 15% in the presence of 250 mM ammonium sulfate. Upon adsorption on a supporting carbon film, these complexes adopted various orientations leading to different enzyme projections. Characteristic dimer (Figure 1B) and monomer (Figure 1D) views were obtained upon alignment, clustering and averaging of 1670 and 1975 molecular images, respectively.

The angular relationships between the three most characteristic dimer views were deduced unambiguously from the previously determined three-dimensional model of the dimeric enzyme (Schultz *et al.*, 1993) and from the position of the internal 2-fold symmetry axis. Figure 1C represents the three orientations of the model corresponding to the dimer views shown in Figure 1B. Two monomer projections (Figure 1D) were selected out of a larger number of views (data not shown) and showed a pseudo-mirror symmetry indicating that they represent two upside down positions of the enzyme. The orientation of the enzyme giving rise to these views could be deduced from their resemblance to half of the 90° dimer view. Interestingly, a 2.5 nm wide and 4 nm long protein density is visible at the dimerization interface (arrows in Figure 1D). This region could not be detected in the dimer due to superimposition. These monomer and dimer views were also obtained upon analysis of immune complexes and were used to locate the antibody interaction site on the three-dimensional model.

The overall shape of an IgG molecule was determined under similar staining, imaging and processing conditions. An average projection of a representative antibody orientation was obtained upon alignment of 358 molecular images (Figure 1E). The IgG molecule was 15 nm in its largest dimension and was divided into three almost identical and slightly elongated domains 5×8 nm in size. These domains represented the Fv and the two Fab fragments connected by a solvent-accessible hinge region.

Immune complexes formed with the anti-A_{135} monoclonal antibody

When the enzyme was incubated in buffer A with subunit A_{135}-specific monoclonal antibodies, characteristic RNA polymerase dimers were observed. The dimer to monomer ratio was not affected by using a 10-fold molar excess of IgG, indicating that the binding of the antibody did not interfere with dimerization. Six hundred dimer images were analyzed and showed the same pattern of views as obtained for the native enzyme, indicating that the orientation of the enzyme was not affected by antibody binding (Table I).

The most frequently occurring 90° and –30° dimer views were analyzed further, and a stain-excluding volume whose size and shape were consistent with those of an IgG molecule was observed to project out in 32 and 37% of the dimers, respectively (Figure 2A, Table I). The binding was found to be specific, since 64% (for the 90° dimer views) and 84% (for the –30° dimer views) of the label clustered into two symmetry-related areas located at both ends of the elongated dimer (Table I). Residual label was distributed equally over the whole contour of the dimer and may correspond to false identification of the IgG molecule or to non-specific binding.

The images of specifically labeled RNA polymerase dimers were averaged to define accurately the antibody interaction site on each projection. Due to the symmetry within the 90° dimer view, the images where the upper RNA polymerase monomer was labeled could be merged with those where antibody bound the lower monomer (Figure 2B, first panel). The density difference map between the labeled and the unlabeled dimer view revealed that the additional stain-excluding volume due to the Fab part of the probe entered the external enzyme contour by a distance of 2–3 nm, indicating that the antibody was superimposed on the enzyme (Figure 2B, second panel). In the case of the –30° dimer views, two independent averages were calculated, depending on whether the upper or the lower monomer was labeled. A stain-excluding area protruding out of the RNA polymerase density was detected in both cases (Figure 2C and D, first panel) and was revealed more clearly on a density difference map between the labeled and an unlabeled dimer view (Figure 2C and D, second panel). The interacting entity had an elongated shape and dimensions of 5×9 nm, which were consistent with those of the Fab part of an IgG molecule (Figure 1E).

The analysis of labeled RNA polymerase dimers thus identified a specific antibody binding site on three different enzyme views. When projected on the three-dimensional enzyme model (Figure 2B, C and D, third panel), the labeled sites merged to a unique location defined at a resolution of 3–4 nm and corresponding to the epitope. The antibody binding site is placed at the rear of a finger-

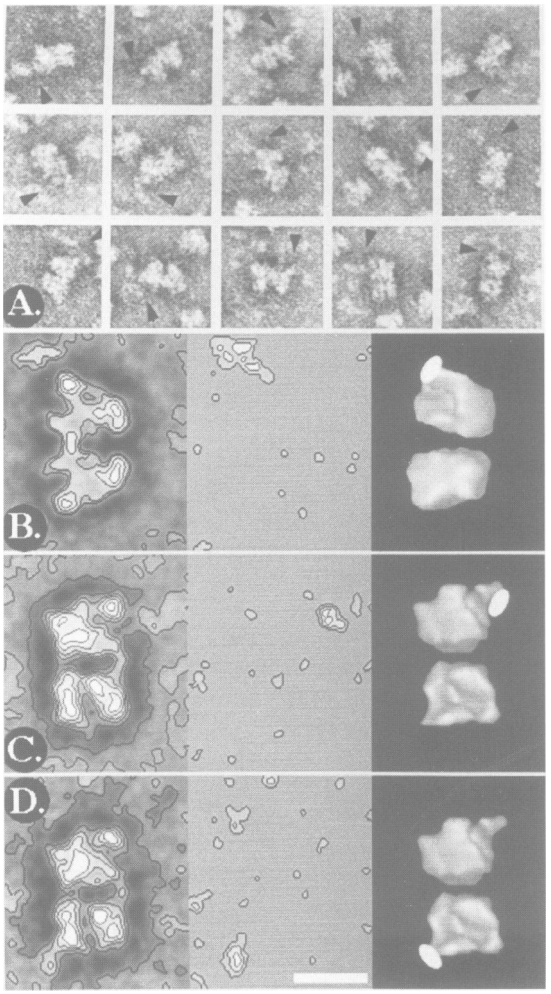

Fig. 2. Analysis of immune complexes formed with the anti-A_{135} monoclonal antibody. (**A**) Gallery of scanning transmission electron micrographs representing antibody-labeled RNA polymerase dimers. The interaction site is indicated by arrowheads. (**B**) Panel 1: average image of labeled RNA polymerase dimers in the +90° orientation. Due to the internal symmetry of the dimer, all the images were transformed to present the label in the upper molecule. Panel 2: difference image between the upper and the lower molecule of the dimer shown in panel 1. The contours correspond to positive differences thresholded at a significance level of 5%. Panel 3: surface representation of the three-dimensional RNA polymerase dimer model oriented so as to correspond to the views represented in panel 1 and on which the antibody interaction site is highlighted by a white dot. (**C**) Panel 1: average image of RNA polymerase dimers in the –30° orientation labeled on the upper molecule. Panel 2: difference image between the labeled dimer view shown in panel 1 and the unlabeled view shown in Figure 1. The contours correspond to positive differences thresholded at a significance level of 5%. Panel 3: surface representation of the three-dimensional RNA polymerase dimer model oriented so as to correspond to the views represented in panel 1 and on which the antibody interaction site is highlighted by a white dot. (**D**) Same representation as in (C) except that the lower monomer is labeled. The bar represents 35 nm in (A) and 12 nm in (B–D).

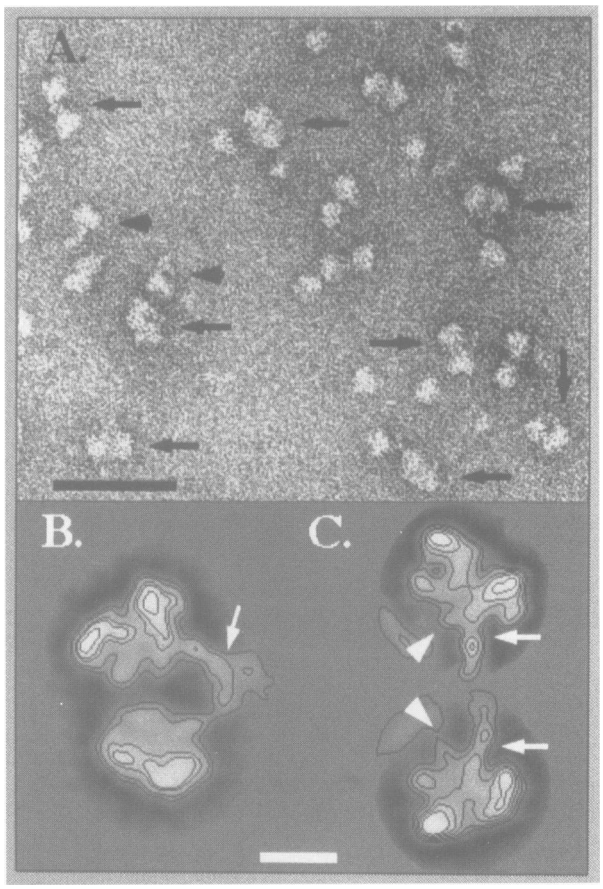

Fig. 3. Analysis of immune complexes formed with the anti-A_{190} monoclonal antibody and adsorbed on a carbon film. (**A**) Transmission electron micrograph showing RNA polymerase molecules incubated with equimolar amounts of antibody. Binary complexes (thick arrowheads) or ternary complexes (thin arrows) correspond respectively to an IgG molecule interacting with one or two RNA polymerase molecules. The bar represents 50 nm. (**B**) Average image of aligned ternary complexes showing the exit site of the antibody and the IgG hinge region (arrow). A better resolution is obtained for the upper RNA polymerase molecule. The antibody interaction site lies close to the external contour of the RNA polymerase projection since the whole length of the Fab arm is observed. (**C**) Average images obtained when the upper and lower monomer images were aligned independently. The two RNA polymerase monomer views are then better defined and are found similar to the unlabeled monomer views shown in Figure 1D. The antibody interaction sites (arrows) are close to but clearly distinct from the protein densities protruding from the dimerization interface (arrowheads). The bar represents 10 nm in (B) and (C).

like stalk, which defines a tunnel, and the end of a 3 nm wide groove (Figure 7).

A library displaying peptides derived from the gene coding for subunit A_{135} was constructed in order to map the epitope on the primary amino acid sequence. The panning was done with the antibody and yielded 40% positive clones from the FUS-C library in immunoblots. Sequencing of 20 positive clones resulted in three different clones showing an overlap of 38 amino acids (Figure 8A). The epitope recognized by the monoclonal antibody covers amino acids 325–362 and is located at 32 residues from the N-terminal border of homology region C (Figure 8B).

Immune complexes formed with the anti-A_{190} monoclonal antibody

When the RNA polymerase preparation was incubated with equimolar amounts of mAb107-9, the dimeric form of the enzyme almost disappeared while two types of immune complexes appeared (Figure 3A). In ternary complexes, the antibody linked two enzyme monomers (Figure 3A, thin arrows), whereas in binary complexes, the IgG molecule interacted with a single RNA polymerase molecule (Figure 3A, thick arrowheads).

A total of 1480 images of ternary complexes were analyzed, 990 of which were selected out for their homogeneous shape with respect to the flexibility of the antibody hinge region. When the aligned images were averaged, the Y-shaped antibody connecting the two RNA polymerase molecules was clearly defined except for the Fv region, which was blurred (Figure 3B). The antibody hinge region (arrow in Figure 3B) was at a distance of 6.2 nm from the contour of the enzyme, indicating that the Fab fragment was not superimposed on the enzyme and that the epitope was close to the outer contour. A more resolutive average was obtained when the labeled monomer images were aligned independently (Figure 3C). The labeled monomer views were similar in shape and dimensions to unlabeled enzyme views (Figure 1D), and related to the 90° dimer projection (Figure 1B). The antibody binding site was located close to, but was clearly distinct from, the protein density at the dimerization interface (arrows in Figure 1D). The peculiar location of the epitope in the dimerization interface accounts for the decreased dimer stability upon antibody binding. The distance between the two epitopes and their relative orientation probably favored the simultaneous binding of both antibody paratopes and may explain the high proportion of ternary complexes.

The identification of the antibody binding site on two upside down enzyme views was not sufficient to locate the epitope unambiguously on the spatial model. To obtain a different view of the labeled enzyme, charged lipid layers were used to modify the RNA polymerase orientation. When lipid-bound enzyme molecules were incubated with antibodies, close packed areas containing the monomeric and dimeric enzyme forms were observed (Figure 4A). An important proportion of monomers, but not of dimers, showed an additional stain-excluding domain (Figure 4A or black dots in Figure 4B) which could arise from the binding of an antibody molecule. The differential labeling of the monomers was in keeping with the observation that dimers dissociated upon antibody interaction. A data set of 806 images of labeled RNA polymerase monomers was analyzed and could be clustered reproducibly into two classes (Figure 4C, 1 and 2), corresponding to two different orientations of the enzyme. A round stain-excluding volume of ~5 nm in diameter is superimposed on the average density of the RNA polymerase (arrows in Figure 4C, 1 and 2). The Y shape of the antibody is not recognized on these average images, probably because, upon drying, the IgG molecule flattens down in random directions. The round shape may thus represent a rotational average of the antibody molecule centered on the epitope. The best fit of these experimental projections with the three-dimensional enzyme model, projected under 44 different orientations, is shown in Figure 4D. The antibody binding site was defined as the center of the superimposed density (Figure 4E).

The analysis of carbon- or lipid-bound immune complexes thus identified the antibody interaction site on three different views of the enzyme. The three labeled sites were projected on the three-dimensional model and merged at the same location on the enzyme surface (Figures 4E and 7), thus attesting to the internal consistency of the data. The A_{190} epitope is located in the dimerization interface within a protein domain facing the domain labeled by the anti-A_{135} probe. The epitope is placed

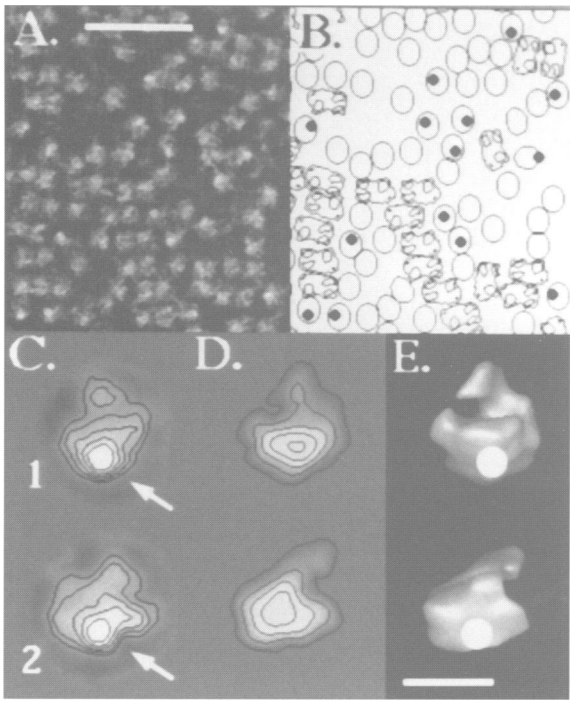

Fig. 4. Analysis of immune complexes formed with the anti-A_{190} monoclonal antibody and interacting with positively charged lipid layers. (**A**) Field of a scanning transmission electron micrograph showing monomeric and dimeric RNA polymerase molecules interacting with a positively charged lipid layer and incubated with monoclonal antibodies mAb107-9. The dimers have started to organize into columns but are not yet crystallized. The labeling, which appears as an additional density superimposed on the enzyme shape, is only observed on monomers. (**B**) Schematic representation of (A). The circles, elongated shapes and black dots show respectively monomers, dimers and the superimposed density due to the antibody. (**C**) Analysis of the labeled monomers defining two different projections (1 and 2) represented as equidensity contours. The additional density appears as a round domain superimposed on the density of the enzyme (arrows). (**D**) Projections of the three-dimensional RNA polymerase model best fitting the labeled projections shown in (C). (**E**) Surface representation of the three-dimensional model of RNA polymerase. The orientations of the model correspond to the projections represented in (D). The labeled site, not resolved in the viewing direction, is highlighted by a white spot. The bar represents 50 nm in (A and B) and 10 nm in (C–E).

at the outside of this groove, close to an extended protein stalk.

A peptide library derived from the gene coding for subunit A_{190} was constructed from pNOY16 in order to map the epitope on the primary amino acid sequence. The panning yielded 80% enzyme-linked immunosorbent assay (ELISA)-positive clones from the FUS-C library. Sequencing of 44 positive colonies resulted in two different clones with an overlapping region of 18 amino acids (Figure 8C). The epitope recognized by the monoclonal antibody encompasses amino acids 544–562 and is located between conserved regions c and d (Figure 8D).

Complexes formed with anti-AC_{19} and anti-AC_{40} polyclonal antibodies

The dimerization of RNA polymerase was not affected by the incubation with subunit AC_{19}- or AC_{40}-specific polyclonal antibodies. Labeled RNA polymerase dimers were therefore analyzed as described above. The inter-

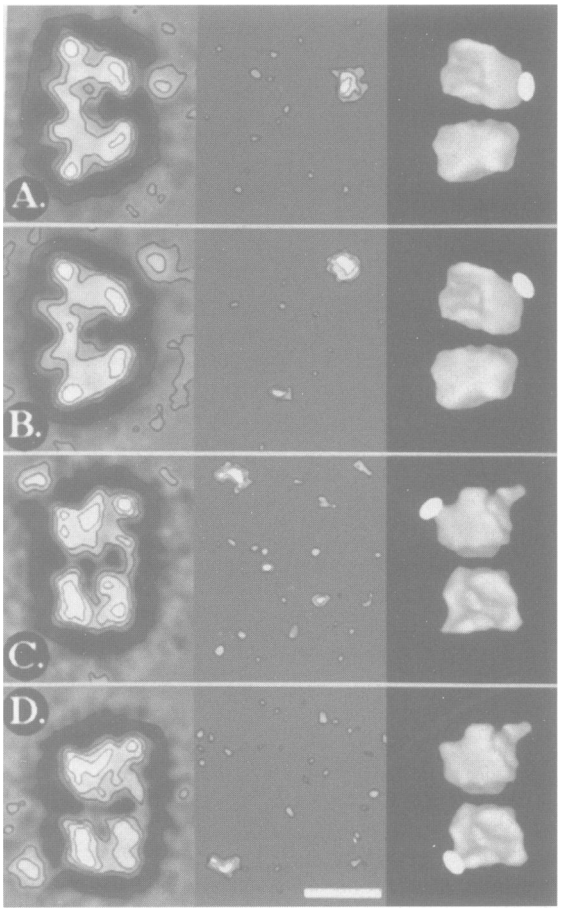

Fig. 5. Analysis of immune complexes formed upon interaction of RNA polymerase dimers with the anti-AC_{40} polyclonal antibody. Representation of the average image, the difference map contoured at 5% significance levels and the surface representation of the three-dimensional model on which the antibody interaction site is highlighted by a white dot for different views of the labeled dimer. (**A**) and (**B**) Two different populations of labeled RNA polymerase dimers in the +90° orientation showing two different interaction sites. (**C**) Dimers in the –30° orientation labeled on the upper monomer. (**D**) Dimers in the –30° orientation labeled on the lower monomer. The bar represents 12 nm.

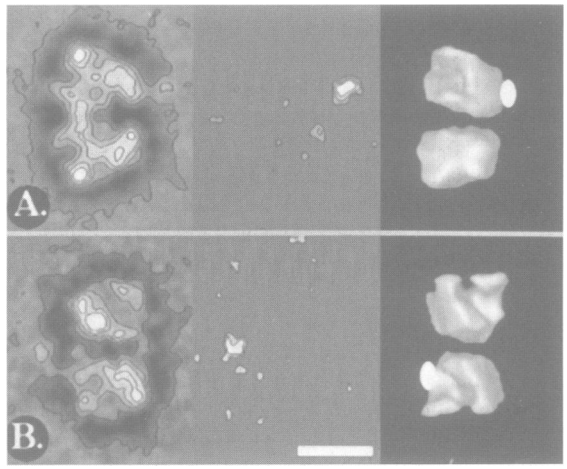

Fig. 6. Analysis of immune complexes formed upon interaction of RNA polymerase dimers with anti-AC_{19} polyclonal antibody. Representation of the average image, the difference map contoured at 5% significance levels and the surface representation of the three-dimensional model on which the antibody interaction site is highlighted by a white dot for different views of the labeled dimer. (**A**) Dimers in the –90° orientation. (**B**) Dimers in the 0° orientation labeled on the lower monomer. The bar represents 12 nm.

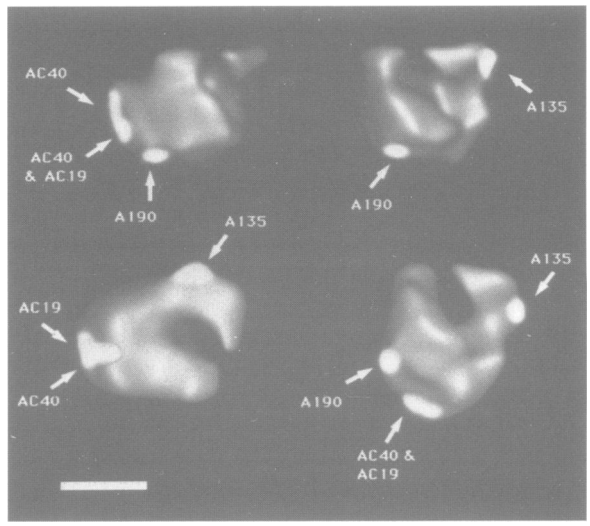

Fig. 7. Representation of the antibody binding sites on the three-dimensional model of yeast RNA polymerase I. The subunit-specific antibody binding sites were determined for each probe on two or three different views of the enzyme and were combined to define their positions on the surface of the model. The bar represents 6.5 nm.

action of the antibody with the enzyme was found to be specific for 63–77% of the complexes (Table I).

The subunit AC_{40}-specific antibodies interacted in the apical region as shown by the average images of the 90° dimer views (Figure 5A and B). In contrast to all other probes used in this study, these antibodies interacted with two distinct binding sites separated by 3–4 nm. This observation suggests that the polyclonal antibodies react with two different epitopes. The analysis of the –30° dimer views labeled with the anti-AC40 antibody identified a specific interaction site on the upper and the lower monomer (Figure 5C–D). When projected on the enzyme model, the site identified on three labeled views merged to a unique location on the surface opposite to the groove, in the apical region of the enzyme (Figure 7).

The average image of the 90° dimer views labeled with the anti-AC_{19} antibody also shows a protein density protruding from the apical region of the enzyme (Figure 6A). The labeled region can be almost superimposed on one of the sites labeled by the subunit AC_{40}-specific probe. The –30° dimer view was underrepresented in the presence of the anti-AC_{19} antibody (Table I) and did not show sufficient specificity (data not shown). In spite of their infrequent occurrence, the labeled 0° dimer views were then analyzed since, by virtue of the internal 2-fold symmetry, the images where the upper monomer was labeled could be merged with those where antibody bound the lower monomer. The IgG interaction site could be identified on the average image of the 0° dimer view (Figure 6B), thus providing a second projection to localize the binding region on the surface of the enzyme. Subunit AC_{19} is almost co-localized with one site labeled with the subunit AC_{40}-specific probe in the apical region of the enzyme (Figure 7).

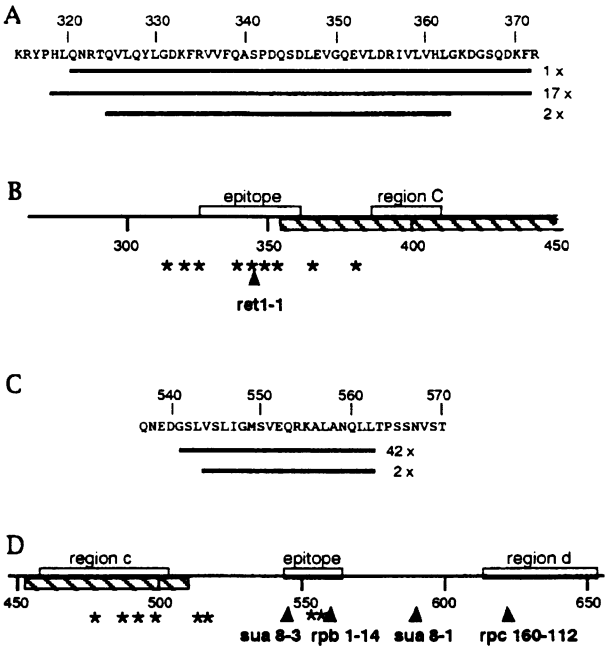

Fig. 8. Sequences of the epitopes recognized by the monoclonal antibodies. (**A**) Amino acid sequence of the epitope recognized by the subunit A_{135}-specific antibody mAb2-3. The bars below the sequence represent the different clones derived from the phage display library and their occurrence is indicated. (**B**) Sequence environment of the mAb2-3 epitope on the A_{135} gene. Mutations described in *E.coli* (*, Landick *et al.*, 1990) or in yeast class III RNA polymerase (ret1-1, James *et al.*, 1991) were represented on this diagram by calculating their corresponding position in the A_{135} gene from the center of conserved region C. (**C**) Amino acid sequence of the epitope recognized by the subunit A_{190}-specific antibody mAb107-9. The bars below the sequence represent the different clones derived from the phage display library and their occurrence is indicated. (**D**) Sequence environment of the mAb107-9 epitope on the A_{190} gene. Mutations described in *E.coli* (*, Weilbaecher *et al.*, 1994), in yeast class II (rpb1-14, Scafe *et al.*, 1990; sua8, Berroteran *et al.*, 1994) or class III (rpc160-112, Dieci *et al.*, 1995) RNA polymerases were represented on this diagram by calculating their corresponding position in the A_{190} gene from the center of conserved region d. Hatched regions in (B) and (D) were described to bind nucleic acid (Allison *et al.*, 1985; Kontermann *et al.*, 1993; Kontermann and Bautz, 1994).

Discussion

The general architecture of multisubunit RNA polymerases is conserved in prokaryotes and eukaryotes (Darst *et al.*, 1991a; Schultz *et al.*, 1993; Polyakov *et al.*, 1995). The global structure of these enzymes is characterized by a groove constituting a putative DNA binding site, and a finger-shaped domain partially occluding the entrance of the groove thus forming a 2.5 nm wide channel. An extended apical region is located on the face opposite to the groove. This structural resemblance indicates that the core subunits, and particularly the β- and β′-like subunits, determine to a large extent the shape of the enzyme. This immunoelectron microscopy study localized subunit-specific sites on the surface of the enzyme. The spatial location of the antibody targets can be correlated with the role of the subunits as studied by biochemical or genetic methods. The structural data thus start to merge into a functional model of the enzyme, especially for the channel region and the apical part of the enzyme.

Function of the finger-like stalk

The channel and groove region were proposed to bind DNA since their width is appropriate to fit a double-stranded template and since their length is consistent with DNase I protection (Darst *et al.*, 1989; Schultz *et al.*, 1993, and references therein). The channel region, which is formed in part by the finger-like domain, shows an overall structural similarity with the envelope of monomeric nucleic acid polymerases (Ollis *et al.*, 1985; Kohlstaedt *et al.*, 1992; Sousa *et al.*, 1993). The envelope of the Klenow fragment of the *E.coli* DNA polymerase can be superimposed almost exactly on the channel region of the prokaryotic RNA polymerase (Darst *et al.*, 1989). The finger-like domain was shown to be flexible in T7 RNA polymerase where it may play a role in enzyme processivity by preventing the dissociation of the template after each reaction cycle (Sousa *et al.*, 1994). In the prokaryotic RNA polymerase, a similar conformationnal change was suggested by comparing the structure of core and holo enzyme (Polyakov *et al.*, 1995). Therefore, the channel region is likely to participate in the active site.

The results reported here support this model since they show that the base of the finger-like stalk, and most probably the stalk itself, is formed by subunit A_{135} which contains important determinants of the active site (Riva *et al.*, 1987; Grachev *et al.*, 1989; Treich *et al.*, 1992). The anti-A_{135} antibody was found to bind at the rear of the finger-like domain. Remarkably, this monoclonal antibody inhibits non-specific transcriptional activity and this inhibition is partially relieved by pre-incubation of the enzyme with DNA (Huet *et al.*, 1982a). The antibody may sterically hinder the binding of DNA. If this interpretation were correct, the DNA would be expected to slide at the base of the stalk. Accordingly, the epitope recognized by the anti-A_{135} antibody was mapped 22 residues away from conserved domain C which was shown to bind DNA (Figure 8B, Allison *et al.*, 1985; Kontermann and Bautz, 1994). Alternatively, the antibody may interfere with a conformational change of the enzyme involving the finger-like stalk. In favor of a two enzyme conformation model is the old observation that only 50% of RNA polymerase I molecules could interact with and were inhibited by the monoclonal antibody. This dual conformation could correspond to an open and closed position of the channel (Sousa *et al.*, 1994; Polyakov *et al.*, 1995).

Several mutations, identified in the bacterial and the yeast class III enzymes, were projected on the A_{135} gene and mapped within or close to the epitope (Figure 8B; Landick *et al.*, 1990; James *et al.*, 1991). Although the amino acid sequence of the epitope is not conserved, the site is sufficiently close to homology region C to consider that mutations with similar phenotypes could exist in the yeast class I enzyme. All mutations in the vicinity of the epitope alter the pausing and/or termination properties of the enzyme. In view of the DNA binding properties postulated for this region, the most plausible explanation for the mutant phenotype is an altered DNA–enzyme interaction whose stability could modulate the elongation–termination equilibrium. We cannot exclude, however, that the nascent RNA, supposedly synthesized in the channel region, interacts close to the epitope and that the termination is affected by altered interactions between the enzyme and the RNA or the heteroduplex.

Role of the apical region

The apical region, opposite the groove, concentrates within reach of 5 nm the antibody interaction sites for the α-like subunit AC_{40}, subunit AC_{19} and amino acids 544–562 of the β′-like subunit A_{190}. The spatial proximity of subunits AC_{40} and AC_{19} is consistent with the extragenic suppression and the two-hybrid experiments which indicated that the two subunits interact (Lalo *et al.*, 1993). These experiments also showed that the smallest RNA polymerase subunit, $ABC_{10\beta}$, which is common to all three enzyme forms, interacts with subunits AC_{40} and AC_{19}. The apical region thus contains at least three different polypeptides in addition to the largest subunit. Previous immunoelectron microscopy studies performed with the *E.coli* enzyme placed α at a location similar to that of subunit AC_{40} (Tichelaar *et al.*, 1983), thus reflecting the sequence similarity found between these subunits (Mann *et al.*, 1987). In contrast to the results obtained with the monoclonal antibodies, the anti-AC_{40} polyclonal antibodies bound to two distinct sites. These two sites could belong to the same polypeptide. The 3–4 nm distance between the sites is consistent with the expected dimensions of a 40 kDa globular molecule. More probably, these results indicate the presence of two AC_{40} subunits forming a dimer, as observed for its homologs, the prokaryotic α subunit (Yura and Ishihama, 1979) and the yeast RNA polymerase II B_{44} subunit (Kolodziej and Young, 1989). The use of monoclonal antibodies should resolve this question.

The position of the α-like subunit relative to the channel region is critical for the orientation of the DNA molecule which is believed to bind in the channel and in the groove. The eubacterial α subunit plays a role in promoter recognition by interacting directly with sequence-specific upstream DNA elements (Ross *et al.*, 1993) and in transcriptional regulation by binding to specific sets of transcription activator proteins (Igarashi and Ishihama, 1991; Kolb *et al.*, 1993; reviewed by Russo and Silhavy, 1992). These functions are mediated by the C-terminal part of the protein which binds DNA as an isolated entity in a region between –42 and –62 bp upstream of the transcriptional start site, which corresponds to a distance of 14–21 nm from the polymerization site if B-form DNA is assumed (Blatter *et al.*, 1994). This value is in good agreement with the shortest distance of 14 ± 3 nm measured on the three-dimensional model between the channel region which is believed to contain the active site and the center of the anti-AC_{40} antibody-labeled region. In this orientation, the downstream DNA would be located in the groove whereas the upstream sequences would interact with the enzyme surface in front of the channel and outside of the groove, which is supported by a distinct DNase protection pattern characterized by a 10 bp repeat (Metzger *et al.*, 1989; Kolb *et al.*, 1993).

In eukaryotes, the general transcription factors required for specific initiation bind to DNA sequences 30 bp upstream of the start site (Wasylyk, 1986). In keeping with the proposed DNA orientation and the documented functions of α in *E.coli*, the enzyme surface in the vicinity of the AC_{40} subunit would constitute a binding interface for these factors. In this respect, the A_{190}-specific epitope, projected on the sequence of the corresponding yeast class II enzyme gene, carries the *sua8-3* suppressor mutation and is close to the *sua8-1* and *sua8-2* mutations (Figure 8D; Berroteran *et al.*, 1994). The *sua8* family of mutations is affected in transcription start site selection, and nearly identical effects are observed for *sua7* suppressors which encode altered forms of TFIIB. It was proposed that the suppressor mutations delineate the TFIIB contact points with the largest subunit of RNA polymerase II. These findings further indicate a role of the apical region in RNA polymerase recruitment and in the initiation of transcription. Image analysis of monomeric RNA polymerases revealed a 2.5 nm wide and 4 nm long protein stalk hidden in the dimerization interface. This structure is probably part of the β′-like subunit since the specific antibody interacts some 3–4 nm away from the base of this stalk. The function of this protein domain is not known but, considering its proximity to the *sua8* mutations and its peculiar shape, a role in contacting the pre-initiation complex cannot be excluded.

The A_{190}-specific epitope maps 62 amino acids residues away from the most highly conserved homology region d containing the motif (Y/F)NADFDGD(E/Q)M(N/A), which is invariant in all multisubunit RNA polymerases. The epitope is placed at an equivalent distance from homology regions c and d. An extensive mutagenesis of that region in yeast RNA polymerase III produced a mutant (rpc160–112) with a reduced elongation rate and a propensity to catalyze a slippage reaction during the early phase of RNA synthesis (Dieci *et al.*, 1995). These results indicated that region d is part of the polymerization site and is therefore predicted to be located close to the channel. The distant location of the epitope relative to the channel is not contradictory, since the ends of a 62 amino acid long peptide can be at a distance of ~9.3 nm when organized in an α-helix.

When projected on the A_{190} subunit gene, several mutations detected in the *E.coli* β′ subunit and affecting transcriptional pausing or termination fall within or close to the epitope (Figure 8; Weilbaecher *et al.*, 1994). These mutants most probably affect the enzymatic reaction by a different mechanism from those detected near the finger-like stalk because of the considerable distance between these two sites. These mutants may have modified RNA binding properties, since several lines of evidence support the idea that the apical region contains an RNA interaction site. Photocross-linking experiments performed in *E.coli* revealed the binding of RNA to the C-terminal domain of the α subunit when the transcript is longer than 25 nucleotides (Liu and Hanna, 1995). Further experiments showed that the α subunit, and therefore the apical region, is the target of regulatory events involving the transcription elongation factor NusA (Liu *et al.*, 1996).

The apical region thus appears to be an essential site for the enzymatic reaction and reflects the pleiotropic functions of the α-like subunits. Beside its role in enzyme assembly, the apical region is believed to interact with the upstream DNA and with basal transcription factors. In the elongation phase, this region is likely to bind the nascent RNA when its length exceeds 25 nucleotides.

Materials and methods

RNA polymerase and antibody purification.

Yeast *Saccharomyces cerevisiae* RNA polymerase I or A was purified and assayed as previously described (Buhler *et al.*, 1980; Huet *et al.*,

1982a). The purified enzyme was stored at –20°C in buffer A [20 mM Tris–HCl, pH 7.4, 50 mM ammonium sulfate, 5 mM $MgCl_2$, 2 mM dithiothreitol (DTT), 20% glycerol] at a concentration of 3 mg/ml.

The monoclonal antibody mAb107-9 directed against the largest subunit A_{190} was raised in mouse by injecting an SDS-treated enzyme. The mouse monoclonal antibody mAb2-3 directed against the second largest subunit A_{135} was obtained by injecting the native enzyme (Huet *et al.*, 1982b). Polyclonal antibodies directed against subunits AC_{40} and AC_{19} were raised in rabbits upon injection of gel-purified subunits. The antibodies were purified by ammonium sulfate precipitation and DEAE-cellulose chromatography and were assayed for their ability to immunoprecipitate the native enzyme (Buhler *et al.*, 1980). The interaction specificity was determined by immunoblotting (Bréant *et al.*, 1983) or spot-immunodetection (Huet *et al.*, 1982b) methods.

Epitope mapping using subunit-specific phage libraries

Epitopes recognized by mAb107-9 and mAb2-3 were mapped using gene-fragment phage display libraries (Petersen *et al.*, 1995). In short, plasmids harboring the genes coding for A_{190} (pNOY16, Wittekind *et al.* 1990) and A_{135} (pNOY80, Yano and Nomura, 1991) were digested with DNase I in the presence of manganese ions to generate DNA fragments between 50 and 300 nucleotides in length. Fragments were ligated with FUS-P and FUS-C linkers (Petersen *et al.* 1995) providing overhangs compatible with the *Sfi*I restrictions sites of the fUSE5 vector (Parmley and Smith, 1988). Library sizes were between 10^5 and 10^6 transformants yielding between 10^9 and 10^{10} transforming units (TUs). Biotinylated antibodies were bound to streptavidin-coated Petri dishes and one round of biopanning was performed using 10^9 TUs (Smith and Scott, 1993). After elution and infection, different dilutions of the cultures were plated to generate single colonies. Detection of positive phages was done by ELISA or colony immunoblot (Petersen *et al.* 1995), resulting in between 40 and 80% positive clones. Single-stranded DNA was prepared from immunopositive colonies and sequenced to determine the amino acid sequence containing the epitope. The specificity of the antibody reaction was analyzed further by Western blotting of either total phage protein or fusion proteins expressed in pDS/RBSII (Hochuli *et al.* 1988).

RNA polymerase–antibody interaction

The binding of mAb107-9 to RNA polymerase I was probed using an ELISA. The titration experiments showed that maximum binding was obtained at an equimolar enzyme to IgG ratio. Electron microscopy observations performed with the same RNA polymerase to antibody ratio showed that 60% of the enzyme was labeled. An equimolar enzyme to antibody ratio was thus used for the other antibodies, and optimal binding was checked by electron microscopy. A 5-fold molar antibody excess was used to label lipid-bound RNA polymerases.

In order to correlate the structural data with immunochemical data, the interaction specificity of the probe has to be maintained during specimen preparation. Allthough the incubations were therefore performed in solution and in equimolar conditions, the absence of competitor protein may lead to non-specific interactions. This possibility is circumvented by the statistical analysis of 400–600 immune complex images. In a first step, the putatively labeled dimers were identified by a stain-excluding domain whose size and shape were consistent with those of an IgG molecule. These images were scrutinized individually to plot the site where the label left the contour of the dimer. The binding was judged as specific when >60% of the label was clustered in <20% of the total contour which corresponds to a signal to noise ratio better than 5. The different dimer views differ by a rotation around their long axis, normal to the dimerization interafce. As an internal control, the area labeled by a given antibody has to be located at the same distance from the 2-fold symmetry axis in all dimer projections.

When antibodies interact with lipid-bound RNA polymerase molecules, the specific site may be hidden and the direct correlation with in solution studies is impossible. The consistency of the results obtained for carbon- or lipid-bound complexes, e.g. the sites labeled in three different views project on the same spatial location indicates, however, that the subunit-specific interaction is preserved in the presence of lipids.

Specimen preparation

In most experiments, immune complexes formed in solution were diluted to a concentration of 20–30 μg/ml in buffer A. Ten microliters of this preparation were placed on a 10 nm thick carbon film previously treated by a glow discharge in air. After 2 min adsorption, the grid was negatively stained with a 2% uranyl acetate solution.

In the case of anti-A_{190} antibodies, positively charged lipid layers were used to change the orientation of the RNA polymerase molecules as described previously (Schultz *et al.*, 1990a). For these experiments, 10 μl of buffer A were placed in a Teflon well 4 mm in diameter and 1 mm deep. The surface of the droplet was coated with 0.5–1 μl of positively charged lipids at a concentration of 0.5 mg/ml. The lipid mixture used contained oleyl alcohol and oleyl trimethyl ammonium at a 4:1 molar ratio. Five microliters of the RNA polymerase suspension diluted to a concentration of 60 μg/ml were injected in the subphase. After 1 h incubation at 18°C in a humid chamber, the subunit-specific antibody was added and incubated for 30 min. The lipid–protein layer was then transferred to a carbon film and negatively stained with a 2% uranyl acetate solution.

Electron microscopy and image processing

In the case of anti-A_{190} antibodies, micrographs were recorded on Kodak SO163 films at a magnification of 50 000 using a Zeiss EM10CR transmission electron microscope operating at 80 kV and at minimal electron dose conditions (<10 electrons/Å^2). The built-in anti-contamination device was used. Electron micrographs were checked by optical diffraction for the absence of astigmatism and for optimal contrast transfer function. The best micrographs were digitized on the microdensitometer developed by the GSTS (Groupement Scientifique de Télédétection Spatiale) and the SERTIT (Service Régional de Traitement d'Image et de Télédétection, Strasbourg) at 25 μm raster size. For all other antibodies, the images were formed on a Vacuum Generator HB5 Scanning Transmission Electron Microscope (STEM) operating at 100 kV. The observations were performed at –140°C using a dedicated cold stage (Homo, 1980). The dark field signal was digitized in real time using the Gatan image acquisition system. Images were recorded with a pixel spacing of 0.42 nm as calibrated using two-dimensional streptavidin crystals (Darst *et al.*, 1991b). Under these conditions, the electron dose was ~50 electrons/Å^2.

Image analysis was performed using the IMAGIC statistical module (Van Heel and Keegstra, 1981). Immune complex subimages, 96×96 pixels in size, were extracted from the original micrographs by interactive selection. A circular mask with a radius of 40 pixels was applied. The mean intensity of each subimage was set to zero and its internal variance was normalized to 10. The images were spatial band pass filtered over 1/1.1 nm^{-1} to reduce high frequency noise and below 1/11 nm^{-1} to minimize low frequency perturbations such as stain heterogeneity. Double direct alignment procedures were used to align the band pass-filtered images in rotation and translation (Saxton, 1980) against alignment references that were contoured by hand on the displayed image. Multivariate statistical data compression (van Heel and Frank, 1981) and automatic clustering procedures (van Heel, 1989) were used to describe the variability of the image data set on those pixels located inside an interactively created mask. Density differences between average images of the labeled and the unlabeled enzyme were calculated, the differences were normalized by the square root of the sum of the variances of the averages and the normalized differences were thresholded at 1.96 which represents the 5% significance level if normality is assumed (Schultz *et al.*, 1990b).

Acknowledgements

We thank V.Mallouh for support in image processing and J.C.Homo for help with electron microscopes. This work was supported by funds from the Institut National de la Santé et de la Recherche Médicale, the Centre National de la Recherche Scientifique, the Centre Hospitalier Universitaire Régional, the E.E.C. Science Program grant No. SC1-CT91-0702 and the Human Frontier Science Organization grant No. RG 498/93.

References

Allison,L.A., Moyle,M., Shales,M. and Ingles,C.J. (1985) Extensive homology among the largest subunits of eukaryotic and prokaryotic RNA polymerases. *Cell*, **42**, 599–610.

Bartholomew,B., Durkovich,D., Kassavetis,G.A. and Geiduschek,E.P. (1993) Orientation and topography of RNA polymerase III in transcription complexes. *Mol. Cell. Biol.*, **13**, 942–952.

Bartolomei,M.S. and Corden,J.L. (1987) Localization of an α-amanitin resistance mutation in the gene encoding the largest subunit of mouse RNA polymerase II. *Mol. Cell. Biol.*, **7**, 586–594.

Berroteran,R.W., Ware,D.E. and Hampsey,M. (1994) The *sua8* suppressors of *Saccharomyces cerevisiae* encode replacements of conserved residues within the largest subunit of RNA polymerase II

and affect transcription start site selection similarly to *sua7* (TFIIB) mutations. *Mol. Cell. Biol.*, **14**, 226–237.

Blatter,E.E., Ross,W., Tang,H., Gourse,R.L. and Ebright,R.H. (1994) Domain organization of RNA polymerase subunit: C-terminal 85 amino-acids constitude a domain capable of dimerization and DNA binding. *Cell*, **78**, 889–896.

Boisset,N., Radermacher,M., Grassucci,R., Taveau,J.-C., Liu,W., Lamy,J., Frank,J. and Lamy,J.N. (1993) Three-dimensional immunoelectron microscopy of scorpion hemocyanin labeled with a monoclonal Fab fragment. *J. Struct. Biol.*, **111**, 234–244.

Borukhov,S., Lee,J. and Goldfarb,A. (1991) Mapping of a contact for the RNA 3′ terminus in the largest subunit of RNA polymerase. *J. Biol. Chem.*, **266**, 23921–23926.

Bréant,B., Huet,J., Sentenac,A. and Fromageot,P. (1983) Analysis of yeast RNA polymerases with subunit-specific antibodies. *J. Biol. Chem.*, **258**, 11968–11973.

Buhler,J.-M., Huet,J., Davies,K.E., Sentenac,A. and Fromageot,P. (1980) Immunological studies of yeast nuclear RNA polymerases at the subunit level. *J. Biol. Chem.*, **255**, 9949–9954.

Corden,J.L., Cadena,D.L., Ahearn,J.M. and Dahmus,M.E. (1985) A unique structure at the carboxyl terminus of the largest subunit of eukaryotic RNA polymerases II. *Proc. Natl Acad. Sci. USA*, **82**, 7934–7938.

Coulter,D.E. and Greenleaf,A.L. (1985) A mutation in the largest subunit of RNA polymerase II alters RNA chain elongation *in vitro*. *J. Biol. Chem.*, **260**, 13190–13198.

Darst,S.A., Kubalec,E.W. and Kornberg,R.D. (1989) Three-dimensional structure of *Escherichia coli* RNA polymerase holoenzyme determined by electron crystallography. *Nature*, **340**, 730–732.

Darst,S.A., Edwards,A.M., Kubalek,E.W. and Kornberg,R.D. (1991a) Three-dimensional structure of yeast RNA polymerase II at 16 Å resolution. *Cell*, **66**, 121–128.

Darst,S.A., Ahlers,M., Meller,P.H., Kubalec,E.W., Blankenburg,R., Ribi,H.O., Ringsdorf,H. and Kornberg,R.D. (1991b) Two-dimensional crystals of streptavidin on biotinylated lipid layers and their interactions with biotinylated macromolecules. *Biophys. J.*, **59**, 387–396.

Dequard-Chablat,M., Riva,M., Carles,C. and Sentenac,A. (1991) RPC19, the gene for a subunit common to yeast RNA polymerases A (I) and C (III). *J. Biol. Chem.*, **266**, 15300–15307.

de Mercoyrol,L., Job,C. and Job,D. (1989) Studies on the inhibition by α-amanitin of single-step addition reactions and productive RNA synthesis catalysed by wheat-germ RNA polymerase II. *Biochem. J.*, **258**, 165–169.

Dieci,G., Hermann-Le Denmat,S., Lukhtanov,E., Thuriaux,P., Werner,M. and Sentenac,A. (1995) A universally conserved region of the largest subunit participates in the active site of RNA polymerase III. *EMBO J.*, **14**, 3766–3776.

Grachev,M.A., Kolocheva,T.I., Lukhtanov,E.A. and Mustaev,A.A. (1987) Studies of the functional topography of *Escherichia coli* RNA polymerase. *Eur. J. Biochem.*, **163**, 113–121.

Grachev,M.A., Lukhtanov,E.A., Mustaev,A.A., Zaychikov,E.F., Abdukayumov,M.N., Rabinov,I.V., Richter,V.I., Skoblov,Y.S. and Chistyakov,P.G. (1989) Studies on the functional topography of *Escherichia coli* RNA polymerase. A method for localization of the sites of affinity labeling. *Eur. J. Biochem.*, **180**, 577–585.

Gundelfinger,E.D. (1983) Interaction of nucleic acids with the DNA-dependent RNA polymerases of *Drosophila*. *FEBS Lett.*, **157**, 133–138.

Hekmatpanah,D.S. and Young,R.A. (1991) Mutations in a conserved region of RNA polymerase II influence the accuracy of mRNA start site selection. *Mol. Cell. Biol.*, **11**, 5781–5791.

Hochuli,E., Bannwarth,W., Döbeli,H., Gentz,R. and Stüber,D. (1988) Genetic approach to facilitate purification of recombinant proteins with a novel metal chelate adsorbent. *Bio/Technology*, **6**, 1321–1325.

Homo,J.C. (1980) Micro-cryostat for high resolution electron microscope specimen stage. *Electron Microsc.*, **1**, 92–93.

Horikoshi,M., Sekimizu,K. and Natori,S. (1985) Conformational change of DNA binding subunit of RNA polymerase II on binding to DNA. *Biochem. Biophys. Res. Commun.*, **129**, 141–147.

Huet,J., Phalente,H., Buttin,G., Sentenac,A. and Fromageot,P. (1982a) Probing yeast RNA polymerases subunits with monospecific antibodies. *EMBO J.*, **1**, 1193–1198.

Huet,J., Sentenac,A. and Fromageot,P. (1982b) Spot-immunodetection of conserved determinants in eukaryotic RNA polymerases. *J. Biol. Chem.*, **257**, 2613–2618.

Huet,J., Schnabel,R., Sentenac,A. and Zillig,W. (1983) Archaebacteria and eukaryotes possess DNA dependent RNA polymerases of a common type. *EMBO J.*, **2**, 1291–1294.

Huet,J., Riva,M., Sentenac,A. and Fromageot,P. (1985) Yeast RNA polymerase and its subunits. Specific antibodies as structural and functional probes. *J. Biol. Chem.*, **260**, 15304–15310.

Igarashi,K. and Ishihama,A. (1991) Bipartite functional map of the *E.coli* RNA polymerase alpha subunit: involvement of the C-terminal region in transcription activation by cAMP-CRP. *Cell*, **65**, 1015–1022.

James,P., Whelen,S. and Hall,B.D. (1991) The RET1 gene of yeast encodes the second-largest subunit of RNA polymerase III. *J. Biol. Chem.*, **266**, 5616–5624.

Kohlstaedt,L.A., Wang,J., Freidman,J.M., Rice,P.A. and Steitz,T.A. (1992) Crystal structure at 3.5 Å resolution of HIV-1 reverse transcriptase complexed with an inhibitor. *Science*, **256**, 1783–1790.

Kolb,A., Igarashi,K., Ishihama,A., Lavigne,M., Buckle,M. and Buc,H. (1993) *Escherichia coli* RNA polymerase, deleted in the C-terminal part of its alpha-subunit, interacts differently with the cAMP–CRP complex at the lacP11 and at the galP1 promoter. *Nucleic Acids Res.*, **21**, 319–326.

Kolodziej,P.A. and Young,R.A. (1989) The RNA polymerase II subunit RPB3 is an essential component of the mRNA transcription apparatus. *Mol. Cell. Biol.*, **9**, 5387–5394.

Kontermann,R.E. and Bautz,E.K.F. (1994) Nucleic acid binding regions of the second-largest subunit of *Drosophila* RNA polymerase II identified by southwestern blotting. *FEBS Lett.*, **344**, 166–170.

Kontermann,R.E., Kobor,M. and Bautz,E.K.F. (1993) Identification of a nucleic acid-binding region within the largest subunit of *Drosophila melanogaster* RNA polymerase II. *Protein Sci.*, **2**, 223–230.

Lalo,D., Carles,C., Sentenac,A. and Thuriaux,P. (1993) Interactions between three common subunits of yeast RNA polymerases I and III. *Proc. Natl Acad. Sci. USA*, **90**, 5524–5528.

Landick,R., Stewart,J. and Lee,D.E. (1990) Amino-acid changes in conserved regions of the β-subunit of *Escherichia-coli* RNA polymerase alter transcription pausing and termination. *Genes Dev.*, **4**, 1623–1636.

Liu,K. and Hanna,M.M. (1995) NusA interferes with interaction between the nascent RNA and the C-terminal domain of the alpha subunit of the *E.coli* transcription complexes. *Proc. Natl Acad. Sci. USA*, **92**, 5012–5016.

Liu,K., Zhang,Y., Severinov,K., Das,A. and Hanna,M.M. (1996) Role of *Escherichia coli* RNA polymerase alpha subunit in modulation of pausing, termination and anti-termination by the transcription elongation factor NusA. *EMBO J.*, **15**, 150–161.

Lotti,M., Noah,M., Stöffler-Meilicke,M. and Stöffler,G. (1989) Localization of proteins L4, L5, L20 and L25 on the ribosomal surface by immuno-electron microscopy. *Mol. Gen. Genet.*, **216**, 245–253.

Mann,C., Buhler,J.-M., Treich,I. and Sentenac,A. (1987) RPC40, a unique gene for a subunit shared between yeast RNA polymerases A and C. *Cell*, **48**, 627–637.

Martindale,D.W. (1990) A conjugation specific gene (*vnjC*) from *Tetrahymena* encodes a protein homologous to yeast RNA polymerase subunits (RPB3, RPC40) and similar to a portion of the prokaryotic RNA polymerase subunit (rpoA). *Nucleic Acids Res.*, **18**, 2953–2959.

Mémet,S., Gouy,M., Marck,C., Sentenac,A. and Buhler,J.-M. (1988) *RPA190*, the gene coding for the largest subunit of yeast RNA polymerase A. *J. Biol. Chem.*, **263**, 2830–2839.

Metzger,W., Schickor,P. and Heumann,H. (1989) A cinematographic view of *Escherichia coli* RNA polymerase translocation. *EMBO J.*, **8**, 2745–2754.

Ollis,D.L. Brick,P., Hamlin,R., Xuong,N.G. and Steitz,T.A. (1985) Structure of a large fragment of *Escherichia coli* DNA polymerase I complexed with dTMP. *Nature*, **313**, 762–766.

Parmley,S.F. and Smith,G.P. (1988) Antibody-selectable filamentous fd phage vectors: affinity purification of target genes. *Gene*, **73**, 305–318.

Petersen,G., Song,D., Hügle-Dörr,B., Oldenburg,I. and Bautz,E.K.F. (1995) Mapping of linear epitopes recognized by monoclonal antibodies with gene-fragment phage display libraries. *Mol. Gen. Genet.*, **249**, 425–431.

Polyakov,A., Severinova,E. and Darst,S. (1995) Three-dimensional structure of *E.coli* core RNA polymerase: promoter binding and elongation conformations of the enzyme. *Cell*, **83**, 365–373.

Riva,M., Schaffner,A.R., Sentenac,A., Hartmann,G.R., Mustaev,A.A., Zaychikov,E.F. and Grachev,M.A. (1987) Active site labeling of the RNA polymerases A, B and C from yeast. *J. Biol. Chem.*, **262**, 14377–14380.

Rose,K.M., Maguire,K.A., Wurpel,J.N.D., Setler,D.A. and Marquez,E.D. (1983) Monoclonal antibodies directed against mammalian RNA polymerase I. Identification of the catalytic center. *J. Biol. Chem.*, **258**, 12976–12981.

Ross,W., Gosink,K.K., Salomon,J., Igarashi,K., Zou,C., Ishihama,A., Severinov,K. and Gourse,R.L. (1993) A third recognition element in bacterial promoters: DNA binding by the alpha subunit of RNA polymerase. *Science*, **262**, 1407–1413.

Russo,F.D. and Silhavy,T.J. (1992) Alpha: the Cinderella subunit of RNA polymerase. *J. Biol. Chem.*, **267**, 14515–14518.

Saxton,W.O. (1980) Digital processing of electron images: a survey of motivations and methods. In Brederoo,P. and Boom,G. (eds), *Proceedings of the 7th European Congress on Electron Microscopy: The Hague*. Vol. 2, pp. 682–689.

Scafe,C., Martin,C., Nonet,M., Podos,S., Okamura,S. and Young,R.A. (1990) Conditional mutations occur predominantly in highly conserved residues of RNA polymerase II subunits. *Mol. Cell. Biol.*, **10**, 1270–1275.

Schultz,P., Célia,H., Riva,M., Colin,P., Darst,S.A., Kornberg,R.D., Sentenac,A. and Oudet,P. (1990a) Two-dimensional crystals of yeast RNA polymerase A. *J. Mol. Biol.*, **216**, 353–362.

Schultz,P., Nobelis,P., Colin,P., Louys,M., Huet,J., Sentenac,A. and Oudet,P. (1990b) Electron microscopic study of yeast RNA polymerase A: analysis of single molecular images. *Chromosoma*, **99**, 196–204.

Schultz,P., Célia,H., Riva,M., Sentenac,A. and Oudet,P. (1993) Three-dimensional model of yeast RNA polymerase I determined by electron microscopy of two-dimensional crystals. *EMBO J.*, **12**, 2601–2607.

Smith,G.P. and Scott,J.K. (1993) Libraries of peptides and proteins displayed on filamentous phage. *Methods Enzymol.*, **217**, 228–257.

Sousa,R., Chung,Y.J., Rose,J.P. and Wang,B.C. (1993) Crystal structure of bacteriophage T7 RNA polymerase at 3.3 Å resolution. *Nature*, **364**, 593–599.

Sousa,R., Rose,J.P. and Wang,B.C. (1994) The thumb's knuckle. Flexibility in the thumb subdomain of T7 RNA polymerase is revealed by the structure of a chimeric T7/T3 RNA polymerase. *J. Mol. Biol.*, **244**, 6–12.

Sweetzer,D., Nonet,M. and Joung,R. (1987) Prokaryotic and eukaryotic RNA polymerases have homologous core subunits. *Proc. Natl Acad. Sci. USA*, **84**, 1192–1196.

Thuriaux,P. and Sentenac,A. (1992) Yeast nuclear RNA polymerases. In Jones,E.W., Pringle,J.R. and Broach,J.R. (eds), *The Molecular and Cellular Biology of the Yeast Saccharomyces: Gene Expression*. Cold Spring Harbor Laboratory Press, Cold Spring Harbor, NY, vol. 2, pp. 1–98.

Tichelaar,W., Schutter,W.G., Arnberg,A.C., Van Bruggen,E.F.J. and Stender,W. (1983) The quaternary structure of *Escherichia coli* RNA polymerase studied with (scanning) transmission (immuno) electron microscopy. *Eur. J. Biochem.*, **135**, 263–269.

Treich,I., Riva,M. and Sentenac,A. (1991) Zinc-binding subunits of yeast RNA polymerases. *J. Biol. Chem.*, **266**, 21971–21976.

Treich,I., Carles,C., Sentenac,A. and Riva,M. (1992) Determination of lysine residues affinity labeled in the active site of yeast RNA polymerase II (B) by mutagenesis. *Nucleic Acids Res.*, **20**, 4721–4725.

Van Heel,M. (1989) Classification of very large electron microscopical image data sets. *Optik*, **82**, 114–126.

Van Heel,M. and Frank,J. (1981) Use of multivariate statistics in analysing the images of biological macromolecules. *Ultramicroscopy*, **6**, 187–194.

Van Heel,M. and Keegstra,W. (1981) IMAGIC: a fast, flexible and friendly image analysis software system. *Ultramicroscopy*, **7**, 113–130.

Wasylyk,B. (1986) Promoter elements of eukaryotic protein-coding genes. In Reeck,G.R., Goodwin,G.H. and Puigdomenech,P. (eds), *Chromosomal Proteins and Gene Expression*. Plenum Press, New York, pp. 103–119.

Weilbaecher,R., Hebron,C., Feng,G. and Landick,R. (1994) Termination-altering amino acid substitutions in the β′ subunit of *Escherichia coli* RNA polymerase identify regions in RNA chain elongation. *Genes Dev.*, **8**, 2913–2927.

Wittekind,M., Kolb,J.M., Dodd,J., Yamagishi,M., Mémet,S., Buhler,J.M. and Nomura,M. (1990) Isolation and characterization of temperature sensitive mutations in *RPA190*, the gene encoding the largest subunit of RNA polymerase I from *Saccharomyces cerevisiae*. *Mol. Cell. Biol.*, **10**, 2049–2056.

Woychik,N.A., McKune,K., Lane,W.S. and Young,R.A. (1993) Yeast RNA polymerase II subunit RPB11 is related to a subunit shared by RNA polymerase I and III. *Gene Expression*, **3**, 77–82.

Yano,R. and Nomura,M. (1991) Suppressor analysis of temperature-sensitive mutations of the largest subunit of RNA polymerase I in *Saccharomyces cerevisiae*: a suppressor gene encodes the second-largest subunit of RNA polymerase I. *Mol. Cell. Biol.*, **11**, 754–764.

Yura,T. and Ishihama,A. (1979) Genetics of bacterial RNA polymerase. *Annu. Rev. Genet.*, **13**, 59–97.

Received on September 6, 1995; revised on April 18,1996

Note added in proof

Recent crosslinking studies mapped contacts between the 3′ terminus of the nascent transcript and the β′ subunit from *E.coli* RNA polymerase within the corresponding sequence of the mAb107-9 epitope [Markovtsov,V., Mustaev,A. and Goldfarb,A. (1996) Protein–RNA interactions in the active center of transcription elongation complex. *Proc. Natl Acad. Sci. USA*, **93**, 3221–3226] thus confirming the involvement of this region in RNA binding.